Available online at www.sciencedirect.com
SCIENCE DIRECT®
Biochemical and Biophysical Research Communications 322 (2004) 100–104
BBRC
www.elsevier.com/locate/ybbrc

Structural bioinformatics study of PNP from *Schistosoma mansoni*

Nelson José Freitas da Silveira[a], Hugo Brandão Uchôa[a], Fernanda Canduri[a,d], José Henrique Pereira[a], João Carlos Camera Jr.[a], Luiz Augusto Basso[b], Mário Sergio Palma[c,d], Diógenes Santiago Santos[e,*], Walter Filgueira de Azevedo Jr.[a,d,*]

[a] *Department of Physics, UNESP, São José do Rio Preto, SP 15054-000, Brazil*
[b] *Rede Brasileira de Pesquisas em Tuberculose, Department of Molecular Biology and Biotechnology, UFRGS, Porto Alegre, RS 91501-970, Brazil*
[c] *Laboratory of Structural Biology and Zoochemistry, Department of Biology, Institute of Biosciences, UNESP, Rio Claro, SP 13506-900, Brazil*
[d] *Center for Applied Toxicology, Instituto Butantan, São Paulo, SP 05503-900, Brazil*
[e] *Center for Research and Development in Molecular, Structural and Functional Molecular Biology, PUCRS 90619-900, Porto Alegre, RS, Brazil*

Received 8 July 2004
Available online 3 August 2004

Abstract

The parasite *Schistosoma mansoni* lacks the de novo pathway for purine biosynthesis and depends on salvage pathways for its purine requirements. Schistosomiasis is endemic in 76 countries and territories and amongst the parasitic diseases ranks second after malaria in terms of social and economic impact and public health importance. The PNP is an attractive target for drug design and it has been submitted to extensive structure-based design. The atomic coordinates of the complex of human PNP with inosine were used as template for starting the modeling of PNP from *S. mansoni* complexed with inosine. Here we describe the model for the complex *Sm*PNP-inosine and correlate the structure with differences in the affinity for inosine presented by human and *S. mansoni* PNPs.

Keywords: Structural bioinformatics; *Schistosoma mansoni*; PNP; Drug design

Schistosomiasis is a major public health problem in the developing World. It is endemic in 76 countries and territories and amongst the parasitic diseases ranks second after malaria in terms of social and economic impact and public health importance [1]. Purine nucleoside phosphorylase (PNP; EC 2.4.2.1) catalyzes the cleavage of the glycosidic bond of ribonucleosides and deoxyribonucleosides of guanine, hypoxanthine, and a number of related nucleoside congeners [2], in the presence of inorganic orthophosphate (P_i) as a second substrate, to generate the purine base and ribose(deoxyribose)-1-phosphate and has previously been described as participating in the purine-salvage pathway in *Schistosoma mansoni* [3]. It has been demonstrated that schistosomes [4], unlike their mammalian hosts, do not have the capacity to synthesize purine nucleosides de novo and depend exclusively upon the salvage pathway for their purine requirements, suggesting that the pathway's component enzymes may represent potential drug targets for novel chemotherapy. More recently, interest in the salvage pathway has been rekindled and it has been suggested that selective inhibitors of PNP from parasites could prevent the spread of parasitic infections [5]. For example, Immucillin-H, a transition-state analogue of PNP, is a potent inhibitor of the enzyme from *Plasmodium falciparum*, thus preventing the utilization of inosine and deoxyinosine as a source hypoxanthine. This indicates that PNP may be a viable target for antimalarial therapy. The major physiological substrates for mammalian PNP are inosine, guanosine, and 2′-deoxyguanosine [6]. The PNP is an attractive target for drug

* Corresponding authors.
E-mail address: walterfa@df.ibilce.unesp.br (W.F. de Azevedo Jr.).

0006-291X/$ - see front matter © 2004 Elsevier Inc. All rights reserved.
doi:10.1016/j.bbrc.2004.07.088

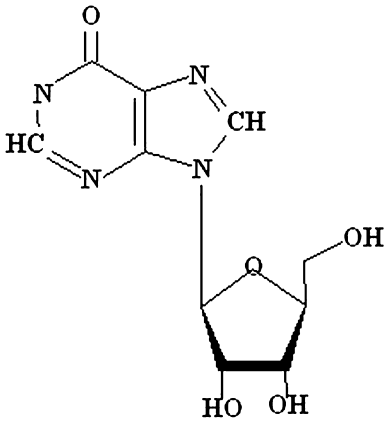

Fig. 1. Molecular structure of *Sm*PNP ligand inosine.

design and it has been submitted to extensive structure-based design [7]. More recently, the three-dimensional structure of human PNP in complex with inosine and ddI (2′,3′-dideoxyinosine) was determined and refined to 2.8 Å resolution (PDB access code: 1RCT) using synchrotron radiation [8]. The atomic coordinates of the complex of human PNP with inosine were used as template. Fig. 1 shows the molecular structure of inosine.

Methods

Molecular modeling. Homology modeling is usually the method of choice when there is a clear relationship of homology between the sequence of a target protein and at least one known structure. This computational technique is based on the assumption that the tertiary structures of two proteins will be similar if their sequences are related, and it is the approach most likely to give accurate results [9].

For modeling of the PNP from *S. mansoni* complexed with inosine we used restrained-based modeling implemented in the program MODELLER [10]. This program is an automated approach to comparative modeling by satisfaction of spatial restraints [11–13]. The modeling procedure begins with an alignment of the sequence to be modeled (target) with related known three-dimensional structures (templates). This alignment is usually the input to the program. The output is a three-dimensional model for the target sequence containing all main-chain and side-chain non-hydrogen atoms. The atomic coordinates of the crystallographic structure of human PNP (PDB access code: 1RCT) solved at 2.8 Å resolution were used as starting model for modeling of the PNP from *S. mansoni* complexed with inosine [8]. The alignment of human PNP (template) and PNP from *S. mansoni* (target) is shown in Fig. 2. Next, the spatial restraints and CHARMM energy terms enforcing proper stereochemistry [14] were combined into an objective function. Finally, the model is obtained by optimizing the objective function in Cartesian space. The optimization is carried out by the use of the variable target function method [10] employing conjugate gradient simulation. Several slightly different models can be calculated by varying the initial structure. A total of 1000 models were generated PNP complexed with inosine, and the final models were selected based on stereochemical quality. All modeling process was performed on a Beowulf cluster, with 16 nodes (AMD Athlon 2100+: BioComp. São José do Rio Preto, SP, Brazil).

Analysis of the model. The overall stereochemical quality of the final model for complex PNP-inosine was assessed by the program PROCHECK [15]. Atomic models were superposed using the program LSQKAB from CCP4 [16]. The cutoff for hydrogen bonds and salt bridges was 3.4 Å. The contact surfaces for the binary complexes were calculated using AREAIMOL and RESAREA [16]. The root mean square deviation (rmsd) differences from ideal geometries for bond lengths and bond angles were calculated with X-PLOR [17,18]. The *G*-factor is essentially just log-odds score based on the observed distributions of the stereochemical parameters. It is computed for the following properties: torsion angles (the analyses provided the observed distributions of ϕ–ψ, χ1–χ2, χ-1, χ-3, χ-4, and ω values for each of the 20 amino acid types) and covalent geometry (for the main-chain bond lengths and bond angles). These values' average was calculated using PROCHECK [15]. The Verify-3D measures the compatibility of a protein model with its sequence, using a 3D profile [19–21].

Results and discussion

Quality of the model

The atomic coordinates of crystallographic structure 1RCT were used as starting model for modeling of the PNP from *S. mansoni*. The atomic coordinates of all waters were removed from the template.

Ramachandran diagram ϕ–ψ plots for the binary complex of PNP from *S. mansoni* (*Sm*PNP) complexed with inosine and human PNP (*Hs*PNP) structure solved to a resolution of 2.8 Å were generated (figure not shown). The Ramachandran plot for the *Hs*PNP

```
                  15            30            45            60            75            90
1RCT:  ---ENGYTYEDYKNTAEWLLSHTKHRPQVAIICGSGLGGLTDKLTQAQIFDYSEIPNFPRSTVPGHAGRLVFGFLNGRACVMMQGRFHMY
SmPNP: MHESVTANIENVKKVAHHIQKLTSIVPEIGIICGSGLGKLADGVKDKITIPYTKIPNFPQTSVVGHSGNLIFGTLSGRKVVVMQGRFHMY
               *  *  *     *   *   ******** * *         *  *****   * ** * * ** * **  * ********

                  105           120           135           150           165           180
1RCT:  EGYPLWKVTFPVRVFHLLGVDTLVVTNAAGGLNPKFEVGDIMLIRDHINLPGFSGQNPLRGPNDERFGDRFPAMSDAYDRTMRQRALSTW
SmPNP: EGYSNDTVALPIRVMKLLGVKILMVSNAAGGLNRSLKLGDFVILKDHIYLPGLGLNNILVGPNQEAFGTRFPALSNAYDRDLRKLAVQVA
       ***    *  * **  ****  * * *******     **     *** ***    * * *** * ** **** * ****  *  *

                  195           210           225           240           255           270
1RCT:  KQMGEQRELQEGTYVMVAGPSFETVAECRVLQKLGADAVGMSTVPEVIVARHCGLRVFGFSLITNKVIMDYESLEKANHEEVLAAGKQAA
SmPNP: EENGFGNLVHQGVYVMNGGPCYETPAECTMLLNMGCDVVGMSTIPEVVIARHCGIQVFAVSLVTNISVLDVESDLKPNHEEVLATGAQRA
          *       * ***  **  ** ***  *   * * ***** ***  *****  **  ** **    * **  * ******* * * *

                  285
1RCT:  QKLEQFVSILMASIPLPDKAS
SmPNP: ELMQSWFEKIIEKLPKD----
                   *
```

Fig. 2. The sequence alignment of human PNP (PDB access code: 1RCT) and PNP from *Schistosoma mansoni* (*Sm*PNP). The sequence of *Sm*PNP shows ~47% of identity with the sequence of *Hs*PNP. The alignment was performed with the program CLUSTAL W [30].

structure was used to compare the overall stereochemical quality of *Sm*PNP model against *Hs*PNP structure solved by biocrystallography. Analysis of the Ramachandran plot of the *Sm*PNP model shows that 93.4% of the residues lie in the most favorable regions and the remaining 5.7% in the additional allowed regions. The same analysis for crystallographic *Hs*PNP structure presents 83.6% of residues in the most favorable, 13.1% additional allowed regions, and 0.8% generously allowed regions. The overall rating for the *Sm*PNP model is slightly poorer than the one obtained for the structure of *Hs*PNP. However, it has over 90% of the residues in the most favorable regions. The rmsd values of bond lengths and bond angles, the average *G*-factor, and Verify 3D values are shown in Table 3.

Overall description

A BLAST search showed that *Sm*PNP is most similar to the mammalian PNPs. The high identity between *Sm*PNP and *Hs*PNP (~47%) classifies *Sm*PNP as a member of the low-molecular-mass PNPs which are homotrimers with an M_r of between 80 and 100 kDa that are specific for the catalysis of 6-oxopurines and their nucleosides. The model of *Sm*PNP complexed with inosine is folded into the typical bilobal structure as was observed for *Hs*PNP structure. The N- and C-terminals show low sequence identity when compared with the human homologues. Furthermore, despite conservation of the phosphate and ribose-1-phosphate-binding subsites, two mutations are observed in the base-binding subsite of the active site. Phe200 and Lys244 in the *Hs*PNP enzyme are replaced by Tyr202 and Ile246 in *Sm*PNP, respectively. These differences suggest the real possibility of designing nucleoside-based inhibitors which are sufficiently selective to be useful antiparasitic agents. They represent the principal stimulus behind investing further effort in structural studies. The core of *Sm*PNP monomer consists of an extended β-sheet. This sheet is surrounded by α-helices. The structure contains an eight-stranded mixed β-sheet and five-stranded mixed β-sheet of both parallel and antiparallel strands, which join to form a distorted β-barrel. These secondary structural elements are linked by extended loops, a characteristic feature of all PNP molecules [2]. Fig. 3 shows a schematic drawing of the complex *Sm*PNP-inosine.

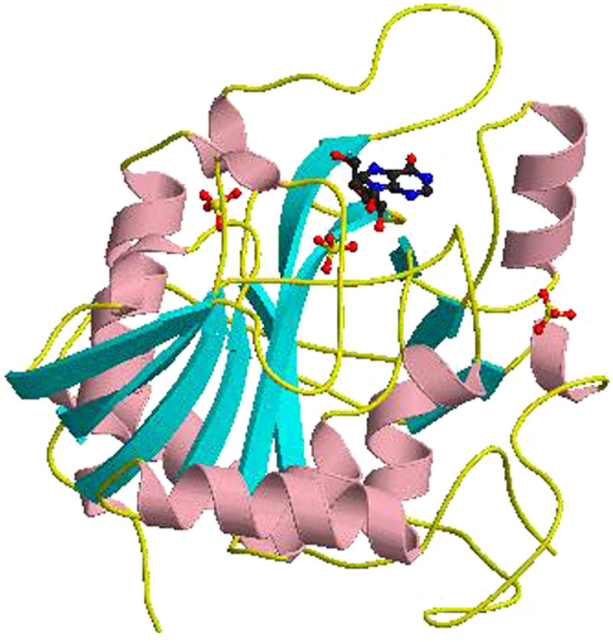

Fig. 3. Ribbon diagram of the PNP of *Schistosoma mansoni* complexed with inosine generated by Molscript [31] and Raster3D [32].

Interactions of inosine with SmPNP

The specificity and affinity between enzyme and its inhibitor depend on directional hydrogen bonds and ionic interactions as well as on shape complementarity of the contact surfaces of both partners [22–24]. Electrostatic interactions including hydrogen bonds and ionic interactions are thought to be major stabilizing forces both for enzyme-substrate interactions [25].

Kinetic studies showed that *Sm*PNP and *Hs*PNP are active against inosine, with a K_M of 7 and 45 μM, respectively [26,27]. A total of eight hydrogen bonds between *Sm*PNP and inosine, in binary model, involving the residues Glu203, His259, Asn245, Met221, and

Table 1
Intermolecular hydrogen bonds between PNP from *Schistosoma mansoni* and inosine

Hydrogen bonds between active site and ligand			
Inosine	*Sm*PNP		Distance (Å)
N1	Glu203	OE1	2.6
N1	Glu203	OE2	3.1
O5S	His259	ND1	2.9
O6	Asn245	ND2	2.9
N7	Asn245	ND2	3.2
N7	Asn245	OD1	2.6
O2S	Met221	N	3.0
O3S	Tyr90	OH	3.0

Table 2
Intermolecular hydrogen bonds between human PNP (PDB access code: 1RCT) and inosine

Hydrogen bonds between active site and ligand			
Inosine	*Hs*PNP		Distance (Å)
N1	Glu201	OE2	2.5
N1	Glu201	OE1	3.1
O5S	His257	ND1	2.9
O6	Asn243	ND2	2.8
N7	Asn243	ND2	3.3
N7	Asn243	OD1	2.5
O2S	Met219	N	3.0
O3S	Tyr88	OH	3.0

Table 3
Summary of structural results for *Sm*PNP and *Hs*PNP

Analysis of the *Sm*PNP and *Hs*PNP								
Proteins	3D profile[a]			*G*-Factor[b]		rmsd from ideal geometry		Contact surface (Å^2)
	Total score	Ideal score	S_{Ideal} score	Torsion angles	Covalent geometry	Bond lengths (Å)	Bond angles (°)	
*Sm*PNP	124.06	130.94	0.95 S	−0.18	−0.35	0.019	3.352	195.0
*Hs*PNP	143.17	131.40	1.09 S	−0.10	0.22	0.015	2.000	189.0

[a] Total score is the sum of the 3D − 1D scores (statistical preferences) of each residue present in protein. Ideal score $S_{Ideal} = \exp(-0.83 + 1.008 \times \ln(L))$; where L is the number of amino acids. S_{Ideal} score is compatibility of the sequence with their 3D structure. It is obtained from Total score/Ideal score. S_{Ideal} score above $0.45S_{Ideal}$.
[b] Ideally, scores should be above −0.5. Values below −1.0 may need investigation.

Tyr90, were observed. For the *Hs*PNP complexed with inosine eight hydrogen bonds involving the residues Glu201, His257, Asn243, Met219, and Tyr88 were observed. Tables 1 and 2 show the intermolecular hydrogen bonds for both structures. The superposition of *Hs*PNP onto *Sm*PNP is shown in Fig. 4. Analysis of contact area between enzyme and ligand in the binary complexes *Sm*PNP-inosine and *Hs*PNP-inosine indicates higher contact for the complex *Sm*PNP-inosine (Table 3). This structural feature is in accordance with the higher affinity of *Sm*PNP for inosine when compared with *Hs*PNP.

The eletrostatic potential surface of the *Hs*PNP-inosine and the model of *Sm*PNP complexed with the same inhibitor was calculated with GRASP [28] (figure not shown). The analysis of the charge distribution of the binding pocket indicates the presence of some charge complementarity between ligand and enzyme (purine-binding site), though most of the binding pocket is hydrophobic (ribose-binding site) (see Fig. 5).

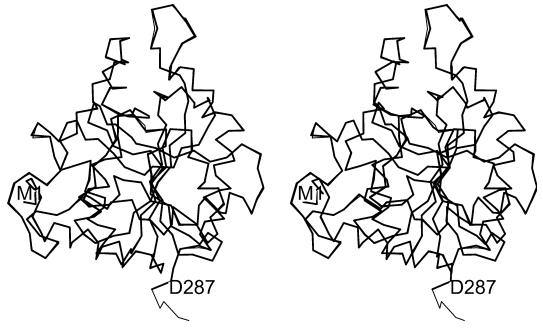

Fig. 4. Stereo view of the C_α–C_α traces of the superimposed structures of *Sm*PNP and *Hs*PNP (1RCT) using LSQKAB from CCP4 [16], which presented an rmsd of 0.14 Å.

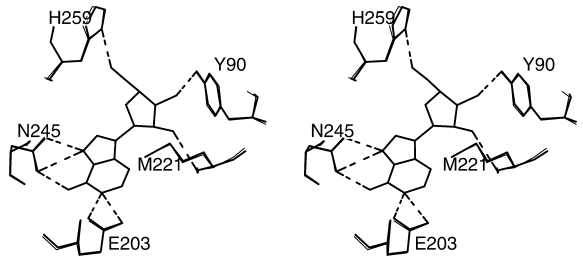

Fig. 5. Stereo view of the interdomain interface region illustrating the binding of inosine in the PNP from *Schistosoma mansoni*.

Conclusion

A further reason for investing on a PNP-based drug-design strategy is the fact that it has been intensively studied as a target for other diseases. For example, potent inhibitors of PNPs may also be useful as immunosuppressive agents as well as in the treatment of gout and in the enhancement of the therapeutic effects of drugs that are purine nucleosides and are therefore cleaved by PNP prior to reaching their target [29]. This work showed that affinity of inosine for *Sm*PNP is higher than that of inosine for *Hs*PNP. Kinetic studies showed that *Sm*PNP and *Hs*PNP are active against inosine, with a K_M of 7 and 45 μM, respectively [26,27]. The complexes show good shape and charge complementarities and exhibit a higher conservation of intermolecular hydrogen bonds (Tables 1 and 2) between PNPs and inosine.

Acknowledgments

This work was supported by grants from FAPESP (SMOLBNet 01/07532-0, 02/04383-7, and 04/00217-0), CNPq, CAPES and Institute of Millennium (CNPq-MCT). W.F.A. (CNPq, 300851/98-7) and M.S.P. (CNPq, 300337/2003-5) are researchers for the Brazilian Council for Scientific and Technological Development.

References

[1] X. Shuhua, M. Tunner, E.K. NáMorgan, J. Utzinger, J. Chollet, R. Bergquist, C. Minggang, Z. Jiang, Recent investigations of artemether, a novel agent form the prevention of schistosomiasis japonica, mansoni and hematobia, Acta Trop. 82 (2002) 175–181.
[2] J.D. Stoeckler, in: R.I. Glazer (Ed.), Developments in Cancer Chemotherapy, CRC Press, Boca Raton, FL, 1984, pp. 35–60.

[3] A.W. Senft, G.W. Crabtree, Pathways of nucleotide metabolism in *Schistosoma mansoni*–VII—inhibition of adenine and guanine nucleotide synthesis by purine analogs in intact worms, Biochem. Pharmacol. 26 (1977) 1847–1855.
[4] A.W. Senft, G.W. Crabtree, Purine metabolism in the schistosomes: potential targets for chemotherapy, Pharmacol. Ther. 20 (3) (1983) 341–356.
[5] A. Bzowska, E. Kulikowska, D. Shugar, Purine nucleoside phosphorylases: properties, functions, and clinical aspects, Pharmacol. Ther. 28 (2000) 349–425.
[6] V.L. Schramm, Enzymatic transition states and transition state analog design, Annu. Rev. Biochem. 67 (1998) 693–720.
[7] W.F. de Azevedo, F. Canduri, D.M. dos Santos, J.H. Pereira, M.V.B. Dias, R.G. Silva, M.A. Mendes, L.A. Basso, M.S. Palma, D.S. Santos, Crystal structure of human PNP complexed with guanine, Biochem. Biophys. Res. Commun. 312 (2003) 767–772.
[8] F. Canduri, D.M. dos Santos, R.G. Silva, M.A. Mendes, L.A. Basso, M.S. Palma, W.F. de Azevedo, D.S. Santos, Structures of human purine nucleoside phosphorylase complexed with inosine and ddI, Biochem. Biophys. Res. Commun. 313 (2004) 907–914.
[9] R. Kroemer, S.W. Doughty, A.J. Robinson, W.G. Richards, Prediction of the three-dimensional structure of human interleukin-7 by homology modeling, Protein Eng. 9 (6) (1996) 493–498.
[10] A. Sali, T.L. Blundell, Comparative protein modelling by satisfaction of spatial restraints, J. Mol. Biol. 234 (1993) 779–815.
[11] A. Sali, J.P. Overington, Deviation of rules for comparative protein modeling from a database of protein structure alignments, Protein Sci. 3 (9) (1994) 1582–1596.
[12] A. Sali, L. Potterton, F. Yuan, H. van Vlijmen, M. Karplus, Evaluation of comparative protein modeling by MODELLER, Proteins 23 (3) (1995) 318–326.
[13] A. Sali, Modeling mutations and homologous proteins, Curr. Opin. Biotechnol. 6 (4) (1995) 437–451.
[14] B.R. Brooks, R.E. Bruccoleri, B.D. Olafson, D.J. States, S. Swaminathan, M. Karplus, CHARMM: a program for macromolecular energy minimization and dynamics calculations, J. Comput. Chem. 4 (1983) 187–217.
[15] R.A. Laskowski, M.W. MacArthur, D.K. Smith, D.T. Jones, E.G. Hutchinson, A.L. Morris, D. Naylor, D.S. Moss, J.M. Thorton, PROCHECK V.3.0 program to check the stereo-chemistry quality of protein structures operating instructions, 1994.
[16] Collaborative Computational Project No. 4, The CCP4 suite: program for protein crystallography, Acta Crystallogr. D 50 (1994) 760–763.
[17] C.D. Schwieters, J.J. Kuszewski, N. Tjandra, G.M. Clore, The Xplor-NIH NMR molecular structure determination package, J. Magn. Res. 160 (2003) 66–74.
[18] A.T. Brünger, X-PLOR Version 3.1: A System for Crystallography and NMR, Yale University Press, New Haven, 1992.
[19] J.U. Bowie, R. Luthy, D. Eisenberg, A method to identify protein sequences that fold into a known three-dimensional structure, Science 253 (1991) 164–170.
[20] R. Luthy, J. Bowie, D. Eisenberg, Assessment of protein models with three-dimensional profiles, Nature 356 (1992) 83–85.
[21] W. Kabsch, C. Sander, Dictionary of protein secondary structure: pattern recognition of hydrogen-bonded and geometrical features, Biopolymers 22 (12) (1983) 2577–2637.
[22] W.F. De Azevedo Jr., S. Leclerc, L. Meijer, L. Havlicek, M. Strrnad, S.-H. Kim, Inhibition of cyclin-dependent kinases by purine analogues: crystal structure of human CDK2 complexed with roscovitine, Eur. J. Biochem. 243 (1997) 518–526.
[23] F. Canduri, L.G.V.L. Teodoro, C.C.B. Lorenzi, V. Hial, R.A.S. Gomes, J. Ruggiero Neto, W.F. De Azevedo Jr., Crystal structure of human uropepsin at 2.45 Å resolution, Acta Crystallogr. D 57 (2001) 277–281.
[24] W.F. De Azevedo Jr., F. Canduri, V. Fadel, L.G.V.L. Teodoro, V. Hial, R.A.S. Gomes, Molecular model for the binary complex of uropepsin and pepstatin, Biochem. Biophys. Res. Commun. 287 (1) (2001) 277–281.
[25] A. Warshel, Computer Modeling of Chemical Reactions in Enzymes and Solutions, Wiley, New York, 1991 pp. 208–228.
[26] H.M. Pereira, A. Cleasby, S.S.D. Pena, G.G.R. Franco, R.C. Garratt, Cloning, expression and preliminary crystallographic studies of the potential drug target purine nucleoside phosphorylase from *Schistosoma mansoni*, Acta Crystallogr. D 59 (2003) 1096–1099.
[27] J.D. Stoeckler, A.F. Poirot, R.M. Smith, E. Parks Jr., S.E. Ealick, K. Takabayashi, M.D. Erion, Biochemistry 26 (1997) 11749–11756.
[28] A. Nicholls, K.A. Sharp, B. Honig, Protein folding and association: insights from the interfacial and thermodynamic properties of hydrocarbons, Proteins 11 (4) (1991) 281–296.
[29] G. Koellner, M. Luic, D. Shugar, W. Saenger, A. Browska, J. Mol. Biol. 265 (1997) 202–216.
[30] J.D. Thompson, D.G. Higgins, T.J. Gibson, CLUSTAL W: improving the sensitivity of progressive multiple sequence alignment through sequence weighting, position-specific gap penalties and weight matrix choice, Nucleic Acids Res. 22 (1994) 4673–4680.
[31] P.J. Kraulis, MOLSCRIPT: a program to produce both detailed and schematic plots of proteins, J. Appl. Crystallogr. 24 (1991) 946–950.
[32] E.A. Merritt, D.J. Bacon, Raster3D: photorealistic molecular graphics, Methods Enzymol. 277 (1997) 505–524.